Determination of the Fe-Ni and Fe-Ni-P Phase Diagrams at Low Temperatures (700 to 300 °C)

A. D. ROMIG, JR. AND J. I. GOLDSTEIN

The $\alpha + \gamma$ two-phase fields of the Fe-Ni and Fe-Ni (P saturated) phase diagrams have been determined in the composition range 0 to 60 wt pct Ni and in the temperature range 700 to 300 °C. The solubility of Ni in $(FeNi)_3P$ was measured in the same temperature range. Homogeneous alloys were austenitized and quenched to form α_2, martensite, then heat treated to form α (ferrite) + γ (austenite). The compositions of the α and γ phases were determined with electron microprobe and scanning transmission electron microscope techniques. Retrograde solubility for the $\alpha/(\alpha + \gamma)$ solvus line was demonstrated experimentally. P was shown to significantly decrease the size of the $\alpha + \gamma$ two-phase field. The maximum solubility of Ni in α is 6.1 ± 0.5 wt pct at 475 °C and 7.8 ± 0.5 wt pct at 450 °C in the Fe-Ni and Fe-Ni (P saturated) phase diagrams, respectively. The solubility of Ni in α is 4.2 ± 0.5 wt pct Ni and 4.9 ± 0.5 wt pct Ni at 300 °C in the Fe-Ni and Fe-Ni (P saturated) phase diagrams. Ternary Fe-Ni-P isothermal sections were constructed between 700 and 300 °C.

THE Widmanstatten pattern observed in iron meteorites is formed by the precipitation and growth of ferrite (α-bcc) in austenite (γ-fcc) during the slow cooling of parent asteroidal bodies to temperatures as low as 300 °C. The major alloying elements in these meteorites are Fe, Ni and P. To describe the development of the Widmanstatten pattern the α-γ phase relations in the Fe-Ni and Fe-Ni-P systems must be known.[1-3] The currently accepted Fe-Ni[4] and Fe-Ni-P[5] phase diagrams have only been experimentally determined to ~500 °C. Therefore, the objective of this study is to determine the α-γ relations to temperatures as low as 300 °C. These data also have practical applicability to various commercial ferrous alloys.

All previously determined Fe-Ni phase diagrams[4,6,7] show a solid solution of γ-FeNi above 912 °C. Below this temperature, pure γ-Fe transforms to the α phase. When sufficient Ni is added to the α phase the two phase $\alpha + \gamma$ mixture develops. Differences between the previously determined Fe-Ni diagrams include the position and shape of the $\alpha/(\alpha + \gamma)$ and $(\alpha + \gamma)/\gamma$ solvus lines.

When an Fe-Ni alloy is cooled in the laboratory from the γ region into the $\alpha + \gamma$ field, the α phase will not nucleate.[4] In meteorites the $\gamma \rightarrow \alpha + \gamma$ transformation does occur because of the presence of P and the extremely slow cooling rate of a few ° C/million years.[8] However, in FeNi alloys, the γ will transform martensitically at low temperatures to a supersaturated bcc phase denoted as α_2. The temperature of the initiation of the $\gamma \rightarrow \alpha_2$ transformation, the M_s temperature, has been measured experimentally as a function of Ni content.[9] The complete transformation to α_2 occurs on reaching M_f which is 25 to 100 °C below M_s. If an alloy with an α_2 structure is tempered in the two-phase field, the γ phase will nucleate and grow. As the Ni-rich γ grows it will deplete the α_2 phase of Ni until the α phase attains its equilibrium composition. This quench and temper cycle has been used to produce the γ and α phases observed in the previous experimental studies of the Fe-Ni phase diagram.

Owen and Sully[6] and Owen and Liu[7] determined the $\alpha + \gamma$ phase field to 300 °C using X-ray powder diffraction techniques. The Owen and Sully[6] data showed retrograde solubility for $\alpha/\alpha + \gamma$ solvus line while the Owen and Liu[5] data indicated that the solubility of Ni in α increased linearly with decreasing temperature. However, inadequacies in their X-ray procedures and the probable lack of equilibrium in the low temperature alloys made accurate positioning of the solvus lines impossible.

The most recently determined Fe-Ni phase diagram, by Goldstein and Ogilvie,[4] was determined to as low as 500 °C. Electron microprobe (EMP) techniques were used to determine the $\alpha + \gamma$ tie-lines from heat treated alloys and diffusion couples. Solubility limits were not

Table I. Alloy Bulk Composition and Results of Homogeneity Study Fe-Ni Alloys

Alloy	wt pct Ni	As-quenched Structure	Homogeneity (±wt pct Ni)
B1	5.13	α_2	0.026
B2	6.20	α_2	0.010
B3	8.12	α_2	0.010
B4	11.91	α_2	0.013
B5	14.23	α_2	0.015
B6	14.56	α_2	0.018
B7	14.71	α_2	0.019
B8	15.22	α_2	0.025
B9	25.50	α_2	0.026
B10	30.65	$\alpha_2 + \gamma$	0.042
B11	40.62	γ	0.042

* Some retained austenite may also be present in the as quenched structures of alloys B1 to B9.

A. D. ROMIG, JR., formerly Research Assistant in Department of Metallurgy & Materials Engineering, Lehigh University, Bethlehem, PA, is now at Sandia Corporation, Albuquerque, NM 87115. J. I. GOLDSTEIN is Professor of Metallurgy, Department of Metallurgy & Materials Engineering, Whitaker Lab #5, Lehigh University, Bethlehem, PA 18015.

Manuscript submitted October 16, 1979.

ISSN 0360-2133/80/0711-1151$00.75/0

Table II. Alloy Bulk Compositions and Results of Homogeneity Study Fe-Ni-P Alloys

Alloy	wt pct Ni	wt pct P	As-quenched Structure	Homogeneity (±wt pct Ni)
T1	5.71	1.27	α_2	0.012
T2	10.12	0.62	α_2	0.019
T3	10.15	0.71	α_2	0.018
T4	11.20	0.98	α_2	0.006
T5	18.75	0.58	α_2	0.027
T6	24.52	0.51	α_2	0.036
T7	27.80	0.63	α_2	0.036
T8	47.97	0.56	γ	0.051

determined below 500 °C because the γ precipitate sizes and interprecipitate distances were smaller than 1 μm, the spatial resolution of the EMP.

The most recent Fe-Ni-P phase diagram is that of Doan and Goldstein.[5] The diagram was determined with EMP techniques, and extends to ~16 wt pct P and to 100 wt pct Ni. Solubility limits were not determined below 550 °C because the γ and $(FeNi)_3P$ precipitates were too small to be analyzed by EMP techniques.

To determine solubility limits from samples with submicron sized precipitates a technique with better spatial resolution is required. The scanning transmission electron microscope (STEM) which has an X-ray spatial resolution of ≈500Å[10] in ferrous alloys has been used in this study. This technique has only recently been suggested for this type of investigation.[11] The increased X-ray spatial resolution of the STEM allows for analysis of α-γ phases at temperatures as low as 300 °C.

PROCEDURE

Alloy Preparation and Heat Treatment

Bulk alloy compositions were chosen to lie within the $\alpha + \gamma$ two phase field of the Goldstein and Ogilvie[4] Fe-Ni diagram or the Doan and Goldstein[5] Fe-Ni-P diagram. The alloys were induction melted from pure elements (99.999 iron, nickel, and phosphorus). The iron and nickel were in the form of 5 mm diam rods and contained less than 0.001 wt pct P. The red phosphorus was added as a powder. The final composition of the alloy was later determined with the electron microprobe. The elemental charge was placed in a 2 ml high-purity Al_2O_3 crucible and was induction melted in a reducing atmosphere (Ar:H_2-20:1 by volume).

Each Fe-Ni and Fe-Ni-P bulk alloy was homogenized in vacuum at 1200 ± 10 °C for at least ten days. After the homogenization the samples were quenched in ice water. Subsequently each sample was held in liquid nitrogen (−196 °C) for at least 15 min to minimize, and hopefully eliminate retained austenite.

To verify homogeneity each alloy was analyzed with the EMP.[12] At least 16 random point counts of Ni were taken on each alloy. The acceptable range of homogeneity was established as ≤ ±0.1 wt pct Ni at the 99 pct confidence level. The average number of Ni and P counts was used to determine the bulk nickel and phosphorus content of the alloys. Tables I and II summarize the composition, homogeneity, and microstructure of the bulk alloys in the as-quenched condition.

The tempering heat treatments were carried out in tube furnaces controlled to within ±0.5 °C. A calibrated Pt-Pt13Rh or chromel-alumel thermocouple was placed next to the samples in the furnace to monitor the actual temperature. Reported temperatures are accurate to ±2 °C. As in the homogenization treatments the alloys were vacuum encapsulated in fused silica tubes and quenched in water by breaking the capsules.

Microchemical Analysis—Electron Microprobe Technique

The heat treated samples were mounted, polished, and etched for metallographic examination. Most samples had structures too fine to resolve optically. Therefore, each sample was also examined with the scanning electron microscope. If the γ precipitates were larger than 2 μm and more than 2 μm apart, the microchemistry was determined with the electron probe. The samples were analyzed with an ARL microprobe, operated at an accelerating potential of 20 kV and a sample current of 0.05 μA on pure Fe. The X-ray data was reduced by the ZAF technique.[13]

Microchemical Analysis—Scanning Transmission Electron Microscopy

All the heat treated samples were examined in the transmission electron microscope (TEM) to establish the presence of suitable thin areas for STEM analysis and to establish that α and γ phases were present in these areas. Self-supporting thin foils were used for the TEM-STEM work. After slicing bulk samples the alloys were chemically thinned to approximately 100 μm with a solution consisting of (by vol) 16 H_2O_2 (30 pct)-3 H_2O-1 HF. A 3 mm disc was then mechanically pierced out of the thinned wafer. The final thinning was accomplished either by an ion beam thinner or an electrojet thinner.

A Commonwealth Scientific IMMI II ion thinner was used for ion beam thinning. The ions were accelerated through a ≈7 kV potential, and the foil was tilted 12 to 14 deg from the beam normal position. Electrojet thinning was accomplished with a Ficionne Jet Thinner and an electrolyte of 3 pct (by vol) perchloric acid in ethanol. A potential of 95 V was used and the solution was cooled to −45 °C with liquid nitrogen. Following jet thinning the foils were placed in the ion thinner for approximately 10 min. This procedure removed any residue deposited on the foil by the electrojet thinning process.

A Philips 300 STEM was used to obtain the X-ray analyses of the thin foils. The X-rays were detected with a Nuclear Semiconductor solid state detector and analyzed with a Tracor Northern 1710 multichannel analyzer. A 60 s counting time was used for each analysis. The instrument was operated at an accelerating voltage of 100 kV and the electron beam size was varied, depending on the resolution desired, between 205 and 390Å. The thin foil was tilted at ≥36 deg and

the α/γ interfaces were oriented approximately parallel to the electron beam.

The X-ray data were converted into weight percents with the Cliff-Lorimer standardless ratio technique[14] as given by the following equation

$$\frac{C_{Fe}}{C_{Ni}} = k_{FeNi}\frac{I_{Fe}}{I_{Ni}} \quad [1]$$

where C_{Fe} and C_{Ni} are the wt pct Fe and Ni present at the analysis point, k_{FeNi} is a proportionality factor which is not a function of composition, and I_{Fe} and I_{Ni} are the net integrated FeK_α and NiK_α peak intensities.

According to Eq. 1 the composition ratio is directly proportional to the intensity ratio. Given k_{FeNi} and the measured values of I_{Fe} and I_{Ni}, C_{Fe} and C_{Ni} can be uniquely determined since $C_{Fe} + C_{Ni} = 1.0$. The prime advantage of the ratio technique is that thickness variations can be ignored and fluctuations in beam intensity do not alter the results. This technique is only applicable if the thin film criterion is satisfied and X-ray absorption and fluorescence effects can be ignored.[15] For most Fe-Ni alloys, the absorption and fluorescence effects can be ignored for foils up to 4000Å thick, which is the limit of electron transparency. Typical foil thicknesses in the area of analysis were 1500Å. For the operating conditions used in these experiments, the X-ray spatial resolution in a 1500Å Fe-Ni foil is approximately 500Å.

To use the ratio technique the value of k_{FeNi} must be known. Five of the alloys listed in Table I containing known bulk Ni contents (5.1 to 40.6 wt pct Ni) were analyzed in the STEM. The results of these measurements yield a k_{FeNi} factor of 0.88 ± 0.05 (99 pct confidence level). The P contents in α and γ are below the detectability limit of the solid state detector. For $(FeNi)_3P$ the compound is assumed to be stoichiometric at ~15.5 wt pct P ($C_{Fe} + C_{Ni} + 0.155 = 1.0$).

Tie-Line Determination

For the appropriate Fe-Ni alloys, concentration profiles of Ni and Fe were measured across two phase α/γ interfaces with the electron probe. For the ternary Fe-Ni-P alloys, concentration profiles for Fe and Ni were measured across α/γ, $\alpha/(FeNi)_3P$ and $\gamma/(FeNi)_3P$ interfaces. A minimum of three concentration profiles were measured for each of two areas in every alloy. In addition, individual electron microprobe analyses of the α, γ, and $(FeNi)_3P$ phases were obtained in appropriate alloys.

Similar procedures were used to analyze the phase compositions in the thin foil samples with the STEM. The thin foil was oriented in the microscope so that the two phase interface was parallel to the incident beam. The electron beam was moved in 1000Å steps across each phase except in the vicinity of the α/γ interface where a step size of 500Å was employed. The concentration profiles were taken perpendicular to the phase

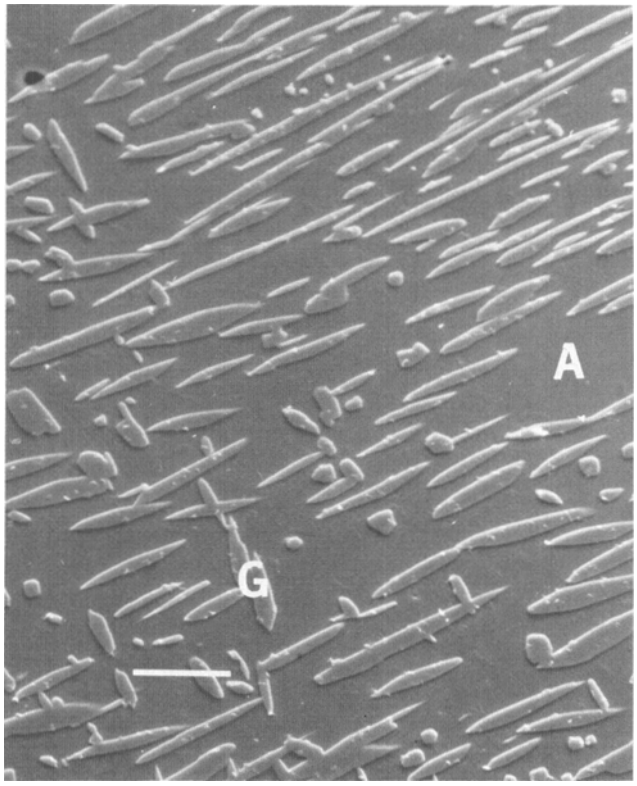

Fig. 1—SEM micrograph of an Fe-15.2 wt pct Ni alloy quenched from 1200 °C into water followed by liquid N_2 (−196 °C). Tempered at 600 °C for 127 days. The structure is austenite (*G*) plates in a ferritic (*A*) matrix. Scale bar = 10 μm.

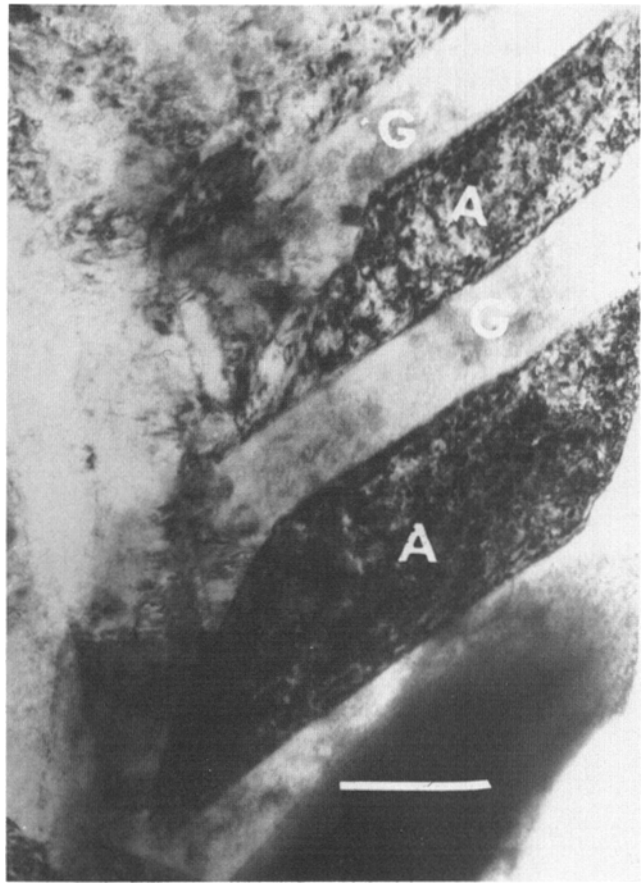

Fig. 2—TEM micrograph of an Fe-14.7 Ni alloy quenched from 1200 °C into water followed by liquid N_2 (−196 °C). Tempered at 500 °C for 127 days. The structure is austenite (*G*) plates in a ferritic (*A*) matrix. Scale bar = 10,000Å.

interfaces and at least three concentration profiles were measured in each sample.

When a binary or ternary alloy was completely equilibrated, the measured composition (by EMP or STEM) of each phase was used to define the two phase tie-line or three phase tie-triangle. For some samples, Ni gradients were measured in the parent α_2 phase. In this case interface compositions were obtained by extrapolating the measured Ni gradients to the interface. These interface values were assumed to represent local equilibrium compositions[16] and were used to define the two phase tie-lines. The applicability of this technique for tie-line determination will be discussed in a later section of the paper.

RESULTS

Microstructure

Figures 1 and 2 show SEM and TEM micrographs of typical $\alpha + \gamma$ structures produced in the heat treated samples. In both the binary and ternary alloys, the γ phase nucleated and grew as platelets or discs in the parent α_2 phase. In the ternary alloys, the phosphides (Ph) nucleated at α/γ interfaces at higher temperatures (700 to 600 °C). At lower temperatures (500 to 300 °C) a few phosphides nucleated at α/γ interfaces, but most phosphides appear as a fine dispersion in the α_2 matrix. Tables III and IV summarize the heat treatment schedule and resultant microstructure of the binary and ternary alloys.

Table III. Fe-Ni Heat Treatments

Temperature (°C)	Composition Ni (wt pct)	Tempering Time (Days)	Structure
670	8.1	74,14	$\alpha + \gamma$ plates
	6.2	74	$\alpha + \gamma$ plates
600	11.9	127	$\alpha + \gamma$ plates
	15.2	127	$\alpha + \gamma$ plates
500	14.7	270	$\alpha + \gamma$ plates
	15.2	270	$\alpha + \gamma$ plates
450	30.7	120	$\alpha + \gamma$ plates
400	25.5	270	$\alpha + \gamma$ plates
	30.7	270	$\alpha + \gamma$ plates
300	25.5	430	$\alpha + \gamma$ plates
	30.6	430	$\alpha + \gamma$ plates
	40.6	430	γ

Table IV. Fe-Ni-P Heat Treatments

Temperature (°C)	Composition Ni (wt pct)	Composition P (wt pct)	Tempering Time (Days)	Structure
700	5.71	1.3	50	$\alpha + \gamma +$ Ph
600	10.12	0.6	124	$\alpha + \gamma +$ Ph
500	18.75	0.6	105	$\alpha + \gamma +$ Ph
400	10.12	0.6	105	$\alpha + \gamma +$ Ph
	18.75	0.6	105	$\alpha + \gamma +$ Ph
300	10.12	0.6	220	$\alpha + \gamma +$ Ph
	18.75	0.6	220	$\alpha + \gamma +$ Ph
	47.97	0.4	220	$\gamma +$ Ph

Microchemistry

Figure 3 shows several concentration profiles measured across α/γ phases in binary Fe-Ni alloys. Figure 3(*a*) shows a concentration profile measured with the

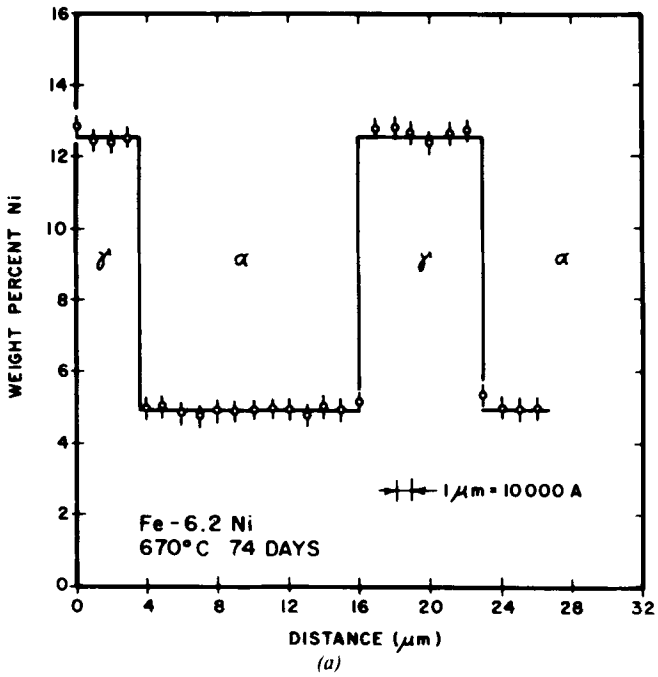

(*a*)

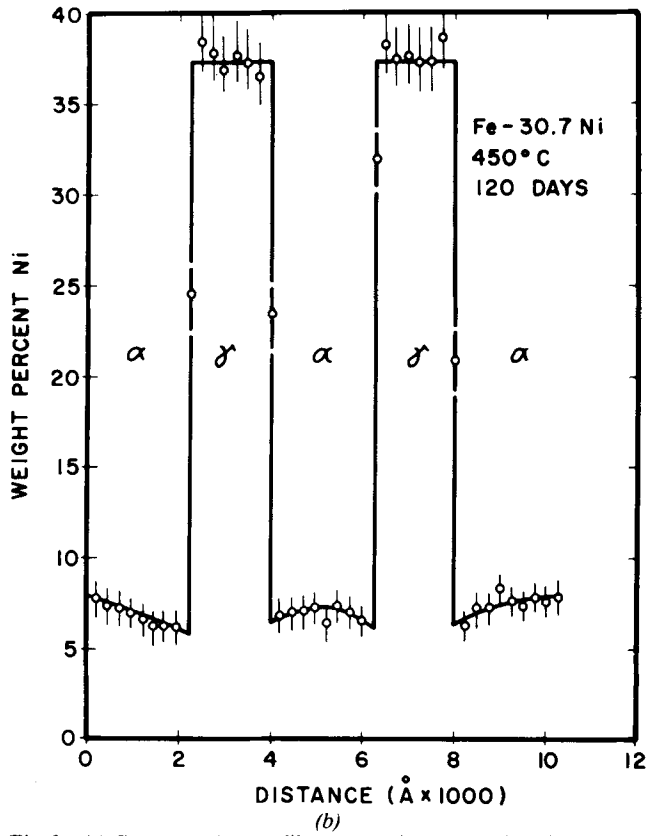

(*b*)

Fig. 3—(*a*) Concentration profile measured on an Fe-6.2 Ni alloy tempered at 670 °C for 74 days. Data taken with the EMP. Step size is 1 μm. Composition of γ: 12.55 ± 0.20 wt pct Ni; composition of α: 4.5 ± 0.20 wt pct Ni, (*b*) concentration profile measured on an Fe-30.7 Ni alloy tempered at 450 °C for 120 days. Data taken with the STEM. Step size is 500Å.

EMP on an Fe-6.2 Ni alloy tempered at 670 °C. The distance between adjacent data points is 1 μm. Figure 3(*b*) shows a concentration profile measured with the STEM on an Fe-30.7 Ni alloy tempered at 450 °C for 120 days. The distance between adjacent data points is 500Å. The alloy treated at 670 °C is fully equilibrated and no concentration gradients are observed in the α phase. The alloy treated at 450 °C is not equilibrated and displays Ni gradients in the α phase. The error bars in Figs. 3(*a*) and (*b*) indicate the error for each probe measurement. The error includes contributions from the counting statistics and the uncertainty in the constant k_{FeNi} used for the calculation of composition.

The Fe-Ni and Fe-Ni-P Phase Diagrams

The two-phase $\alpha + \gamma$ tie-lines and the three-phase tie-triangles were determined from the measured con-

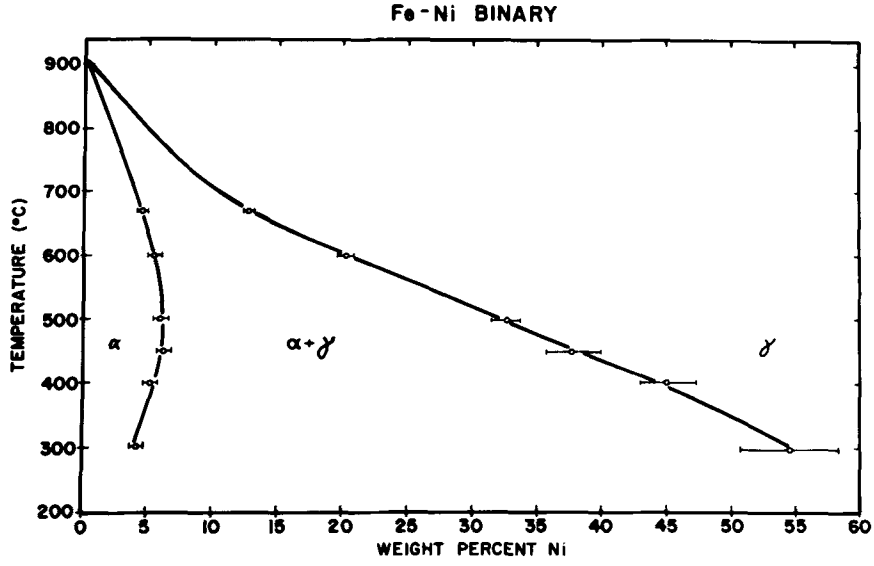

Fig. 4—Fe-Ni binary phase diagram.

Table V. Measured Two Phase Solubility Limits in Fe-Ni Alloys

Temperature (°C)	Technique	Bulk Alloy	Solubility Limits α Phase	Solubility Limits γ Phase
		(wt pct Ni)	wt pct Ni	wt pct Ni
670	EMP,STEM	8.1	4.5 ± 0.2	12.6 ± 0.4
		6.2*	4.5 ± 0.2	12.6 ± 0.4
600	EMP,STEM	11.9	5.4 ± 0.5	20.2 ± 1.4
		15.2	5.4 ± 0.5	20.2 ± 1.4
500	STEM	14.7	5.8 ± 0.4	32.3 ± 2.3
		15.2	5.8 ± 0.4	33.3 ± 2.3
450	STEM	30.7	6.1 ± 0.5	37.6 ± 2.8
400	STEM	25.5	5.1 ± 0.5	44.0 ± 3.1
		30.7*	5.2 ± 0.5	46.0 ± 3.1
300	STEM	25.5	4.3 ± 0.5	54.7 ± 4.1
		30.6*	4.2 ± 0.5	54.5 ± 4.1

* Fully Equilibrated Alloy

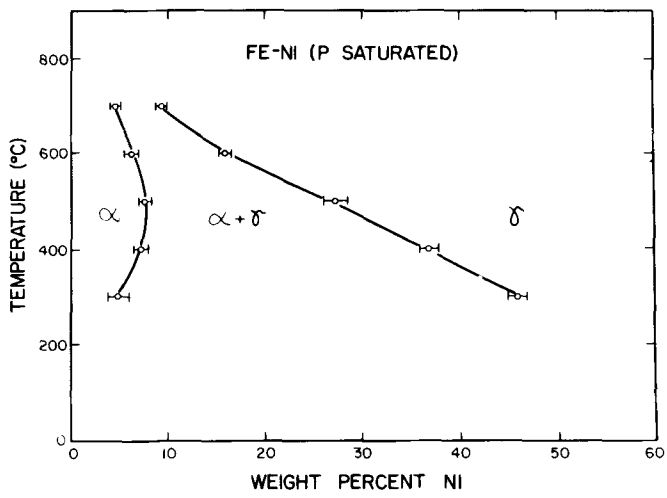

Fig. 5—Fe-Ni (P saturated) pseudobinary phase diagram.

Table VI. Measured Three Phase Solubility Limits in Fe-Ni (P Saturated) Alloys

Temperature (°C)	Technique	Bulk Alloy wt pct Ni	Bulk Alloy wt pct P	Solubility Limits α Phase wt pct Ni	Solubility Limits γ Phase wt pct Ni	$(FeNi)_3P$ Phase wt pct Ni
700	EMP,STEM	5.7*	1.3*	4.5 ± 0.3	9.3 ± 0.5	7.5 ± 0.7
600	EMP,STEM	10.1	0.6	6.1 ± 0.5	15.7 ± 1.1	12.9 ± 1.0
500	STEM	10.1*	0.6*	7.5 ± 0.5	27.3 ± 1.9	31.0 ± 3.0
400	STEM	18.75	0.6	7.2 ± 0.5	37.5 ± 2.6	51.0 ± 5.0
300	STEM	18.75*	0.6*	4.9 ± 0.5	46.0 ± 3.2	71.0 ± 7.0

* Fully Equilibrated Alloy

centration profiles. The concentration profile shown in Fig. 3(*a*) was taken from a fully equilibrated Fe-Ni alloy and the equilibrium tie-line compositions are those of the equilibrated α and γ phases. The concentration profile given in Fig. 3(*b*), however, was from an unequilibrated Fe-Ni alloy heat treated at 450 °C. To obtain the tie-line composition of the α phase, the Ni gradient is extrapolated over a 500Å distance to the α/γ

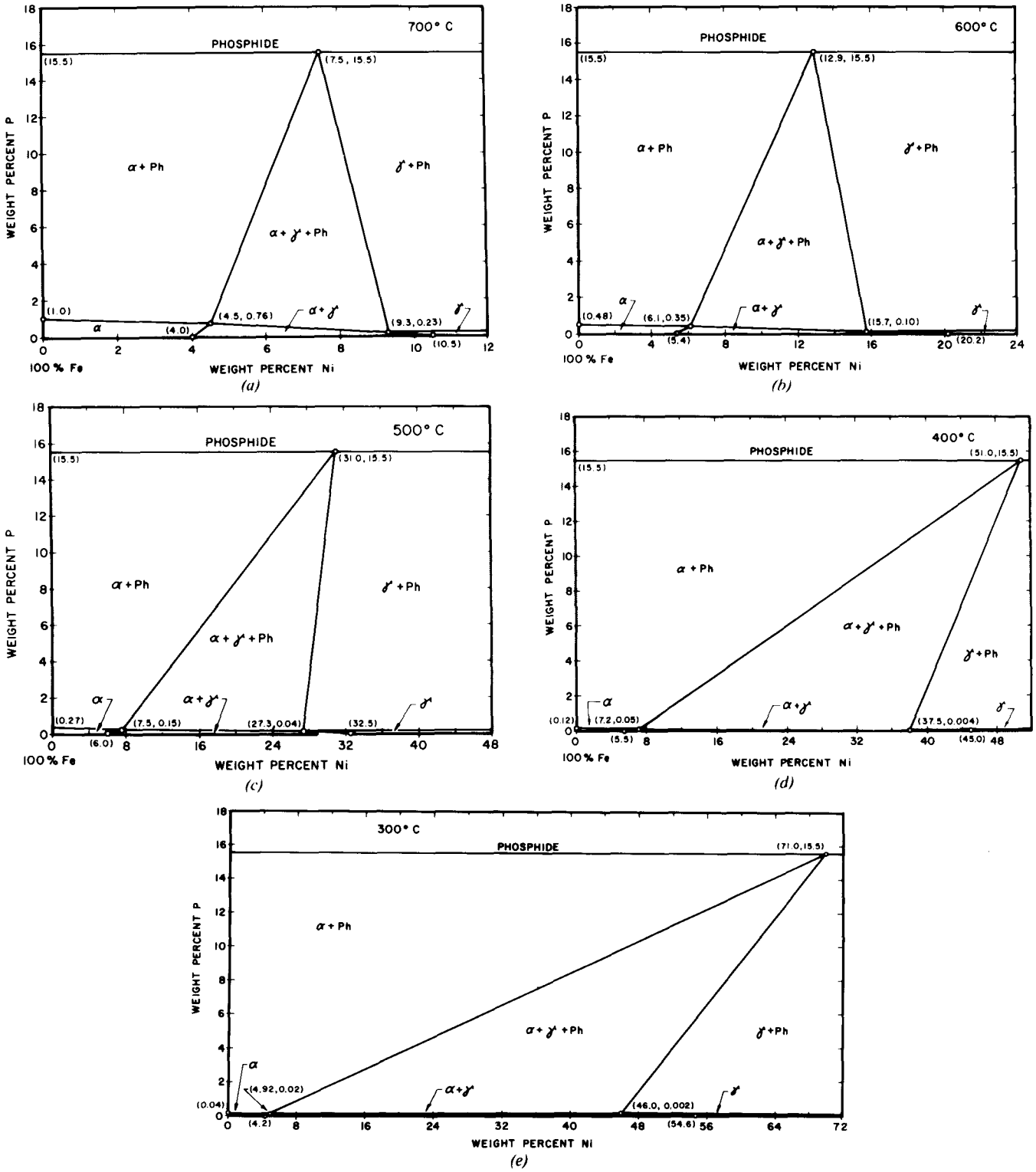

Fig. 6—(*a*) Isothermal section of the Fe-Ni-P phase diagram at 700 °C, (*b*) isothermal section of the Fe-Ni-P phase diagram at 600 °C, (*c*) isothermal section of the Fe-Ni-P phase diagram at 500 °C, (*d*) isothermal section of the Fe-Ni-P phase diagram at 400 °C, (*e*) isothermal section of the Fe-Ni-P phase diagram at 300 °C.

interface. Since the γ precipitates grow at constant composition under isothermal conditions, the γ phase composition yields the γ endpoint of the α + γ tie-line.

Tables V and VI summarize the experimental two-phase (α + γ) and three-phase (α + γ + Ph) solubility data. The error limits given in Tables V and VI are for a 99 pct confidence level. From the data of Tables V and VI the α + γ field of the Fe-Ni and Fe-Ni (P saturated) phase diagrams were constructed, note Figs. 4 and 5. From the data of Tables V and VI and the P solubilities in α and γ[17] ternary Fe-Ni-P isothermal sections were constructed for P contents up to 18 wt pct. Fig. 6 shows sections for 700, 600, 500, 400, and 300 °C.

DISCUSSION

Assumption of Local Equilibrium at the α/γ Interface

There is direct experimental evidence showing the existence of local equilibrium at the α/γ interfaces in Fe-Ni and Fe-Ni-P alloys. For example, Fig. 3(*a*) shows a concentration profile measured for an Fe-6.2 wt pct Ni alloy which is equilibrated after tempering at 670 °C for 74 days. An Fe-8.12 wt pct Ni alloy was tempered at the same temperature, 670 °C, for only 14 days. The concentration profile shown in Fig. 7 indicates that the alloy has not equilibrated. The STEM analysis of the precipitate γ phase yields the same value as in the equilibrated alloy, 12.6 wt pct Ni. From extrapolation of the Ni concentration gradient in α to the α/γ interface in the 8.12 wt pct Ni alloy, the composition of the α phase is 4.5 ± 0.5 wt pct Ni. This value is statistically indistinguishable from that obtained from the equilibrated alloy (4.5 ± 0.2 wt pct Ni). Therefore the measured tie-line compositions are the same regardless of whether the bulk alloy is equilibrated or not.

From this and other alloy combinations evidence has been accumulated that, over the entire temperature range of interest (700 to 300 °C), any deviation from true equilibrium at the α/γ interfaces in Fe-Ni and Fe-Ni-P is too small to be detected by the electron microprobe or the STEM. Therefore within the sensitivity limits of the analysis techniques employed in this study, a state of local equilibrium exists at two phase interfaces.

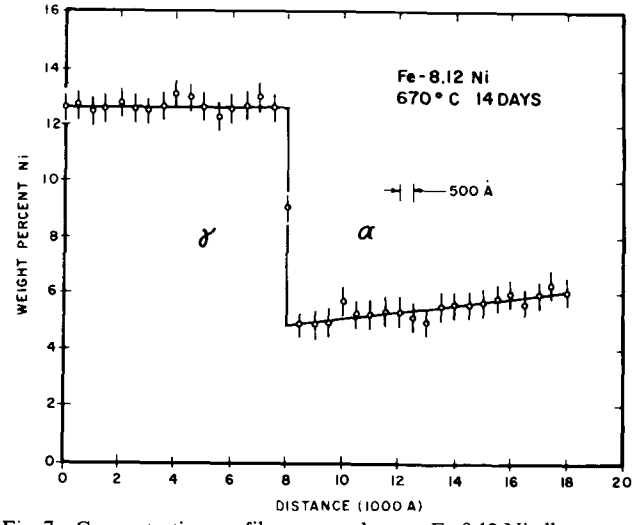

Fig. 7—Concentration profile measured on an Fe-8.12 Ni alloy tempered at 670 °C for 14 days. Data taken with the STEM. Step size is 500Å. Composition of γ: 12.6 ± 1.8 wt pct Ni; composition of α: 4.5 ± 0.5 wt pct Ni. Determined by extrapolating the gradient to the α/γ interface.

Precision and Accuracy of the Electron Microprobe Method

There are several sources of error in the determination of phase diagrams when the electron probe is employed.[12] The errors in the solubility limits determined in this study (Table V and VI) however result mainly from the reproducibility of the various (≥3) microprobe profiles taken across two phase interfaces.

Precision and Accuracy of the Scanning Transmission Electron Microscope Method

There are several sources of error in the determination of the phase solubilities as measured by STEM X-ray microanalysis. These errors include the measurement of the composition at two phase interfaces, the accuracy of the Cliff-Lorimer k_{AB} factor, and the statistical variation in accumulated X-ray counts.

Several factors can lead to uncertainty in determining the concentration of an element at the interface between two phases. The α/γ interface must be parallel to the incident electron beam, or X-rays will be generated from both phases. If one phase overlays another, an average composition will be measured. Extreme care was used to properly orient the foil to minimize this source of uncertainty.

Even if the foil is properly oriented, the Ni concentration gradient must be extrapolated to the two phase interface. The steeper the gradient, the larger is the error in the interface composition. To accurately extrapolate the gradient to the interface, the difference in Ni content between two adjacent data points should not exceed the analytical sensitivity of the STEM analysis (±0.5 wt pct Ni). All the measured gradients were less than this limit. The interface compositions for the α-phase, as determined from all the measured profiles, was reproducible to within ±0.2 wt pct Ni, or 3 to 4 pct relative. The error due to extrapolation of the Ni gradient in α was the most significant error in EMP analysis. However, for STEM analysis, this error is not the most significant. The uncertainty in the value of k_{FeNi} and the low X-ray count rates obtained at each analysis point are the major contributors to the analysis error. The STEM error analysis is outlined below.

The most significant error in STEM X-ray analysis is due to the poor X-ray counting statistics obtained from the X-ray energy dispersive data for the α and γ phases. The X-ray count rates in STEM analysis are so low that the uncertainty in the composition at any analysis point due to counting statistics may be larger than the analytical sensitivity (≈0.5 wt pct Ni).

Experimental observations showed that the STEM X-ray counting statistics obeyed Gaussian behavior.

Hence, $\sigma = \sqrt{N}$ where σ is the standard deviation and N is the number of accumulated counts at each analysis point. At the 3σ confidence level, the error in the number of accumulated counts would be $3\sqrt{N}$. The relative error in the number of counts is $(3\sqrt{N})/N \times 100$, so as N decreases the relative error increases. The Cliff-Lorimer relation (Eq. 1) uses the X-ray ratio, I_{Fe}/I_{Ni}. The relative error for this ratio is the sum of the relative errors for I_{Fe} and I_{Ni}. Therefore the total relative error in C_{Fe}/C_{Ni} for any one measurement would be the sum of the error for I_{Fe}, I_{Ni}, and k_{FeNi}. In the Procedure section it was shown that the error in $k_{FeNi} = 0.88$ is ± 0.05 or ± 6 pct relative at the 99 pct confidence level for the Lehigh Philips 300 TEM/STEM.

For example, one can consider an analysis from a point in the α-phase which contains 6.6 wt pct Ni. For a typical analysis, $I_{Fe} = 10968$ and $I_{Ni} = 870$. At the 3σ confidence level, the relative error for I_{Fe} and I_{Ni} is ~3 pct and ~10 pct, respectively. The relative error for I_{Fe}/I_{Ni} is therefore 13 pct. The total relative error for the composition ratio, C_{Fe}/C_{Ni}, is therefore 6 pct + 13 pct = 19 pct. For a typical γ-phase analysis, where the metal contains 54.6 wt pct Ni, $I_{Fe} = 7576$ and $I_{Ni} = 7985$. The relative error in I_{Fe}/I_{Ni} is 7 pct and therefore the total relative error in C_{Fe}/C_{Ni} is 13 pct. The relative error in C_{Ni} for each measurement was assumed equal to the relative error in C_{Fe}/C_{Ni}. The error bars shown on the data in Fig. 3 were determined using this procedure.

The error in the composition of a tie-line endpoint is substantially smaller than that of an individual measurement since these compositions are determined from n individual determinations. To establish the error for a tie-line endpoint the following procedure was used. The total absolute error in I_{Fe}/I_{Ni} at the 99 pct confidence level would be $\pm(t_{99}^{n-1}S)/\sqrt{n}$, where t_{99}^{n-1} is the Student t value and S is the standard deviation, calculated for n values of the ratio I_{Fe}/I_{Ni}. The relative error in I_{Fe}/I_{Ni} is $(t_{99}^{n-1}S)/\sqrt{n}/(\overline{I_{Fe}/I_{Ni}}) \times 100$, where $\overline{I_{Fe}/I_{Ni}}$ is the average intensity ratio calculated from n values of I_{Fe}/I_{Ni}. In this study, each tie-line endpoint composition was determined from approximately 40 measurements. The typical relative error for 40 values of I_{Fe}/I_{Ni} was 2 to 4 pct. The total relative error in C_{Ni} (tie-line endpoint) would therefore be the sum of 6 pct (from k_{FeNi}) plus 2 to 4 pct (from n values of I_{Fe}/I_{Ni}) which totals 8 to 10 pct. The error in k_{FeNi} and therefore C_{Ni} cannot be reduced below 6 pct, regardless of the value of n. This procedure was used to determine the error for the α, γ, and Ph tie-line endpoint compositions measured with STEM techniques (Tables V and VI). In summary, the error attributable to counting statistics and k_{FeNi} (8 to 10 pct) were much more significant than the error attributable to interface extrapolation (3 to 4 pct).

Comparison of Phase Diagram Results

In Fig. 8 the solubility limits of Ni in α and γ for the binary Fe-Ni determined in this study are compared with the solubility limits determined by Owen and Sully,[6] Owen and Liu,[7] and Goldstein and Ogilvie.[4] The $\alpha/(\alpha + \gamma)$ and $(\alpha + \gamma)/\gamma$ solvus lines determined in this study are significantly different than those of Owen and Sully[6] or Owen and Liu.[7] The solvus lines of Goldstein and Ogilvie[4] as measured to 500 °C are, on the whole, statistically indistinguishable from the solubilities determined in this study.

The Ni solubilities for the Fe-Ni-P ternary system determined in this study agree, within experimental error, with the solubility limits determined by Doan and Goldstein[5] for the α, γ, and $(FeNi)_3P$ phases. This agreement of phase boundary data at >550 °C further demonstrates the ability of the STEM to reproduce the results measured by more conventional electron microprobe techniques.

Several investigators have reported ordered phases including Fe-Ni and $FeNi_3$, in the Fe-Ni system. Kaufman and Nesor[18] have predicted the $\gamma \rightarrow \alpha + FeNi_3$ eutectoid reaction to occur at 345 °C. Billard

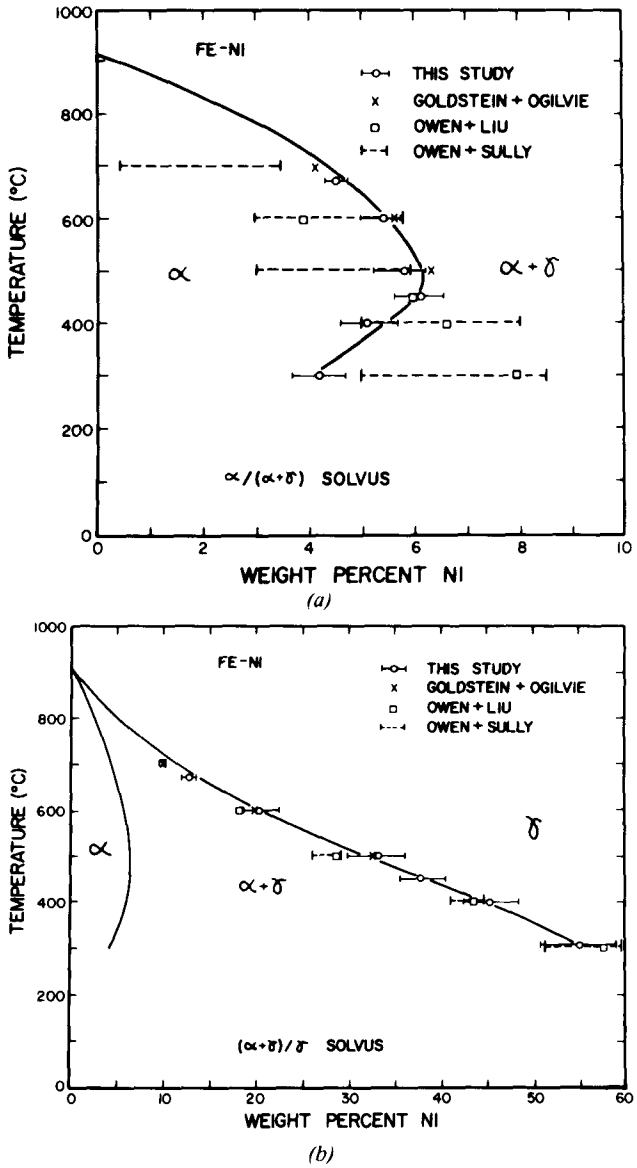

Fig. 8—(*a*) Graphical comparison of the solubility of Ni in α as determined by Owen and Sully,[6] Owen and Liu,[7] Goldstein and Ogilvie,[4] and this study, (*b*) graphical comparison of the solubility of Ni in γ as determined by Owen and Sully,[6] Owen and Liu,[7] Goldstein and Ogilvie,[4] and this study.

and Chamberod[19] have reported that ordered FeNi forms below 320 °C. The FeNi phase was induced by neutron bombardment and its presence detected by Mossbauer spectroscopy. Neither of the ordered phases were detected using electron diffraction techniques as part of this study. The ordered phases may develop at temperatures below 300 °C, may not be easily detected by electron diffraction techniques, or may be kinetically restricted in their formation.

The Effect of P on the $\alpha/(\alpha + \gamma)$ and $(\alpha + \gamma)/\gamma$ Solvus Line

Both the Fe-Ni and Fe-Ni (P saturated) phase diagrams have a retrograde $\alpha/(\alpha + \gamma)$ solvus line. A comparison of Figs. 4 and 5 clearly shows that when the alloy is P saturated, the size of the two phase $\alpha + \gamma$ field is reduced considerably. The magnitude of the effect is very large when one considers the small quantity of P soluble in the metal below 500 °C (<0.15 wt pct P in α and ≤ 0.05 wt pct P in γ). The maximum solubility of Ni in Fe-Ni α is 6.1 ± 0.5 wt pct at ≈475 °C, and the maximum Ni in Fe-Ni (P saturated) α is 7.8 ± 0.5 wt pct at ≈425 °C. The solubility of Ni in α at 300 °C is 4.2 ± 0.5 wt pct and 4.9 ± 0.5 wt pct for Fe-Ni and Fe-Ni (P saturated), respectively. For both the Fe-Ni and Fe-Ni (P saturated) systems, the solubility of Ni in the γ phase increases with decreasing temperature. At 300 °C the solubility of Ni in the γ is 54.6 ± 4.1 wt pct and 46.0 ± 3.2 wt pct for Fe-Ni and Fe-Ni (P saturated), respectively. A qualitative explanation for the effect of P has been proposed by the atomistic-electronic theory of alloy phases.[20] Unfortunately,no quantitative explanation for the effect of P on the solubility limits of the Fe-Ni $\alpha + \gamma$ field can be offered.

Conclusions

The α and γ solubility limits in the Fe-Ni, Fe-Ni (P saturated) and Fe-Ni-P phase diagrams have been determined between 700 and 300 °C. The following facts have been established:

1. The $\alpha/(\alpha + \gamma)$ boundary shows retrograde solubility. The maximum Ni solubility in the α phase occurs at ≈475 °C for Fe-Ni and ≈450 °C for Fe-Ni (P saturated).
2. The solubility of Ni in γ phase for Fe-Ni and Fe-Ni (P saturated) increases with decreasing temperature.
3. P shrinks the size of the $\alpha + \gamma$ field. The maximum solubility of Ni in α is 6.1 ± 0.5 wt pct Ni at ≈475 °C and 7.8 ± 0.5 wt pct Ni at ≈450 °C in the Fe-Ni and Fe-Ni (P saturated) systems, respectively. The solubility of Ni in α is 4.2 ± 0.5 wt pct Ni and 4.9 ± 0.5 wt pct Ni at 300 °C for the Fe-Ni and Fe-Ni (P saturated) systems. The solubility of Ni in γ increases with decreasing temperature to 54.6 ± 4.1 wt pct Ni and 46.0 ± 3.2 wt pct Ni at 300 °C for the Fe-Ni and Fe-Ni (P saturated) systems.
4. The ordered phases, FeNi and $FeNi_3$, were not observed at ≥ 300 °C.
5. "Local equilibrium" was observed to exist at α/γ interfaces from 700 to 300 °C.

ACKNOWLEDGMENTS

The authors wish to acknowledge the advice and counsel of Dr. D. B. Williams of Lehigh and the financial support of this work by the National Science Foundation Grant No. EAR74-22518-A01.

REFERENCES

1. J. I. Goldstein and J. M. Short: *Geochim. Cosmochim. Acta*, 1967, vol. 31, pp. 1001–23.
2. A. E. Moren and J. I. Goldstein: *Earth Planet. Sci. Lett.*, 1978, vol. 40, pp. 151–61.
3. J. Willis and J. T. Wasson: *Earth Planet Sci. Lett.*, 1978, vol. 40, pp. 141–50.
4. J. I. Goldstein and R. E. Ogilvie: *Trans. TMS-AIME*, 1965, vol. 233, pp. 2083–87.
5. A. S. Doan, Jr. and J. I. Goldstein: *Met. Trans.*, 1970, vol. 1, pp. 1759–67.
6. E. A. Owen and A. H. Sully: *Philos. Mag.*, 1939, vol. 27, pp. 614–36.
7. E. A. Owen and Y. H. Liu: *J. Iron Steel Inst.*, 1949, vol. 163, pp. 132–37.
8. J. I. Goldstein and A. S. Doan, Jr.: *Geochim. Cosmochim. Acta*, 1972, vol. 36, pp. 51–69.
9. L. Kaufman and M. Cohen: *Trans. AIME*, 1956, vol. 206, pp. 1393–1401.
10. J. I. Goldstein, D. B. Williams, and A. D. Romig, Jr.: *Workshop in Analytical Electron Microscopy*, pp. 166–69, Cornell University, 1978.
11. A. D. Romig, Jr. and J. I. Goldstein: NBS SP-496, pp. 462–82, 1978.
12. J. I. Goldstein and H. Yakowitz: *Practical Scanning Electron Microscopy—Electron and Ion Microprobe Analyses*, 582 pages, Plenum Press, New York, 1975.
13. J. W. Colby: *Advances in X-ray Analysis, 11*, J. B. Newkirk, G. R. Mallett, and H. G. Pfeiffer, eds., pp. 278–305, Plenum Press, New York, 1968.
14. G. Cliff and G. W. Lorimer: *Proc. 5th European Congress on Electron Microscope*, pp. 140–41, Institute of Physics, London, 1972.
15. J. I. Goldstein, J. L. Costley, G. W. Lorimer, and S. J. B. Reed: *SEM/1977*, O. Johari, ed., pp. 315–24, IIT Research Institute, Chicago, IL, 1977.
16. J. I. Goldstein and R. E. Ogilvie: *Optique des Rayons X et Microanalysis*, R. Castaing, P. Deschampes, J. Philibert, eds., pp. 594–602, Herman, Inc., Paris, 1966.
17. R. S. Clarke, Jr. and J. I. Goldstein: *Smithsonian Contribution to the Earth Sciences*, vol. 21, Smithsonian Institution, Washington, D. C., 1978.
18. L. Kaufman and H. Nesor: *Z. für Metal.*, 1973, vol. 64, pp. 249–58.
19. L. Billard and A. Chamberod: *Solid State Commun.*, 1975, vol. 17, pp. 113–18.
20. A. D. Romig, Jr.: Ph.D. Dissertation, Lehigh University, Bethlehem, PA, 1979.